J. Fluid Mech. (1989), *vol.* 202, *pp.* 201–215
Printed in Great Britain

Cross-sectional convection induced by an insulated boundary in a cylinder

By CHARLES QUON
Physical and Chemical Sciences Branch, Department of Fisheries and Oceans,
Bedford Institute of Oceanography, Dartmouth, N.S., Canada B2Y 4A2

(Received 24 March 1988 and in revised form 6 September 1988)

When a long horizontal cylinder filled with fluid is differentially heated at the end walls at high Rayleigh number, A, the axial flow in the midsection consists of boundary layers at the top and bottom of the cylinder flowing in reverse directions, and the temperature is stably and linearly distributed in the vertical. Both the temperature and the flows are almost independent of the axial dimension. The adiabatic boundary condition on the cylinder requires temperature corrections which can induce cross-section boundary layers on the cylindrical wall and vertical internal boundary layers in the middle. Both types of boundary layers are $O(A^{-\frac{1}{4}})$ in width. Matching different boundary layers at the poles is achieved through additional $A^{-\frac{1}{6}}$ and $A^{-\frac{1}{8}}$ layers. The maximum boundary-layer velocity is calculated to be almost one-quarter of the axial velocity observed in experiments for $A = 10^8$.

1. Introduction

The problem of convection in an insulated horizontal cylinder with differentially heated endwalls has attracted many workers since Hong published his paper in 1977 (Hong 1977; Bejan & Tien 1978; Kimura & Bejan 1980*a*, *b*; Shih 1981; Schiroky & Rosenberger 1984*a*, *b*; Smutek *et al.* 1985, amongst others). These authors have used experimental, analytical and numerical techniques in their studies, and have covered a wide range of Rayleigh numbers, from 10^3 to 10^9. The practical application of this problem in crystal growth in the semiconductor industry and in heat transfer in nuclear reactors has been emphasized in all the works mentioned above. It seems that the primary objectives of these studies are to determine the overall heat transport from one end of the cylinder to the other. Bejan & Tien (1978) were the only authors to have analysed the secondary cross-sectional flows at axial positions sufficiently far away from the endwalls that these flows can be considered independent of the axial dimension. Bejan & Tien studied the low-Rayleigh-number limit, and expanded the stream function and temperature in powers of the Rayleigh number in the way used by Batchelor (1954) in his analysis of low-Rayleigh-number convection in a differentially heated rectangular cavity. In this paper, we shall consider the cross-sectional flows in the other limit, when the Rayleigh number approaches infinity. It appears that none of the studies cited above has addressed this particular problem.

2. Axial flows and temperature distribution at large Rayleigh number

Experiments at high Rayleigh number (Kimura & Bejan 1980*a*; Schiroky & Rosenberg 1984*a*) show that the flows in the vertical axial plane are very similar to those in a differentially heated rectangular cavity, studied by Elder (1965), Gill (1966), Quon (1972), de Vahl Davis (1983) and others. (Also, see Quon 1983*b* and de Vahl Davis & Jones 1983 for a more complete list of references.) Especially relevant to the flows in a long cylinder are the works of Cormack, Leal & Imberger (1974*a*), Cormack, Leal & Seinfeld (1974*b*), Imberger (1974), Bejan, Al-Homoud & Imberger (1981), Simpkins & Dudderar (1981), and Simpkins & Chen (1986) for natural convection in a shallow cavity. Observations also show that at high Rayleigh number, the boundary-layer flows are dominant along both the endwalls and the cylindrical wall. The fluid flows up a thin boundary layer next to the hot end, and then axially along the upper inner cylindrical surface in a second thin layer. After reaching the opposite end of the cylinder, the fluid sinks along the cold wall and then reverses its axial flow direction along another boundary layer on the lower cylindrical surface to complete the circuit. The axial flow in the interior is infinestimal. The three-dimensional temperature distribution is very complex. However, if the cylinder is sufficiently long, the temperature distribution in the cross-section over a large portion of the cylindrical interior can be considered two-dimensional, as a function of x and y, or r and ϕ, only. As shown in the experiments, the fluid is gravitationally stable with an almost linear vertical temperature gradient (Kimura & Bejan 1980*a*). The heat source and sink are provided by the axial boundary layers at the top and bottom of the cylinder where the temperatures almost attain the respective values at the endwalls. Since the temperature in the interior is a function of y only, say $T = y$, y being the vertical coordinate (see figure 1), T cannot meet the adiabatic boundary condition $\partial T/\partial r = 0$ (in fact, the argument holds for any arbitrary temperature function of x and y). In order to satisfy this boundary condition, there must be boundary-layer corrections in temperature, which in turn generate some cross-sectional boundary-layer flows along the curved surface. The problem is very similar to that considered by Quon (1976, 1983*a*), and some of the solutions from the previous studies can be applied here to advantage. The mechanism that induces the boundary-layer flow was originally proposed by Phillips (1970) and Wunsch (1970) as a mixing process along oceanic boundaries. They studied the flows induced along a straight, slanted, impermeable boundary in a fluid with a stable, linear stratification.

3. Statement of the problem

We shall assume a stably stratified fluid enclosed in a cylindrical container as illustrated in figure 1. Note that if the flow is two-dimensional, the final steady state has to be motionless and isothermal because of the adiabatic boundary condition on the cylindrical wall. However, if we assume a forced axial flow supplying heat at the top and draining off heat at the bottom of the cylinder as thermal source and sink, the linearly stratified state is a physically realizable one. For concreteness, we shall accept this as an approximation to the zero-order state obtained from experiments.

The governing equations of motion and energy are the two-dimensional Navier–Stokes equation and the heat transport equation. If we non-dimensionalize the equations with lengthscale a, the radius of the cylinder, with characteristic velocity $U = \kappa/a$, or characteristic stream function κ, and with characteristic

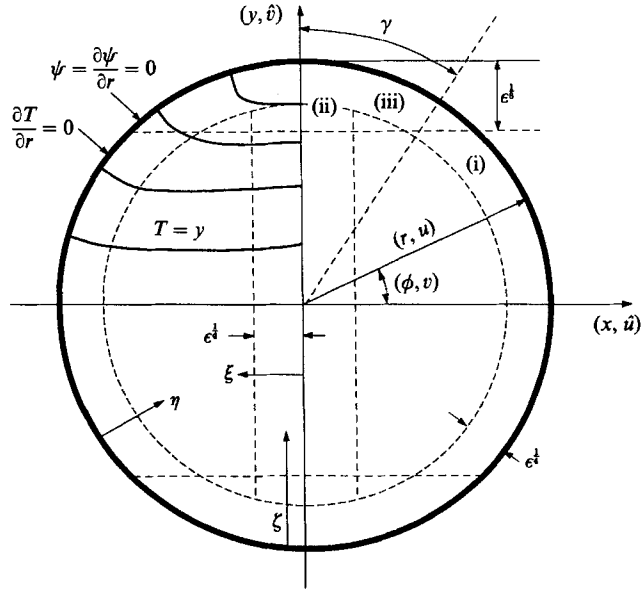

FIGURE 1. The physical system and coordinates.

temperature $\frac{1}{2}\Delta T = \frac{1}{2}(T_2 - T_1)$, where κ is the thermal diffusivity of the fluid, T_2 the temperature at the top, and T_1 the temperature at the bottom, then the non-dimensional governing equations for steady states are as follows (see Quon (1983*a*) for details of argument; much of the discussion there also applies here):

$$\epsilon\nabla^4\Psi + \cos\phi\frac{\partial T}{\partial r} - \sin\phi\, r^{-1}\frac{\partial T}{\partial\phi} = O[\epsilon\sigma^{-1}J(\nabla^2\Psi, \Psi)], \tag{1}$$

$$\nabla^2 T - J(\Psi, T) = 0, \tag{2}$$

with the following boundary conditions;

$$\frac{\partial T}{\partial r} = 0, \quad \Psi = \frac{\partial\Psi}{\partial r} = 0 \quad \text{at} \quad r = 1,$$

where Ψ is the Stoke's stream function, and the radial and azimuthal velocities are respectively defined as $u = r^{-1}\partial\psi/\partial\phi$, and $v = -\partial\psi/\partial r$. In (1) and (2)

$$J(f,g) = r^{-1}\left(\frac{\partial f}{\partial r}\frac{\partial g}{\partial\phi} - \frac{\partial f}{\partial\phi}\frac{\partial g}{\partial r}\right), \quad \nabla^2 = \left(r^{-1}\frac{\partial}{\partial r}\frac{r\partial}{\partial r} - r^{-2}\frac{\partial^2}{\partial\phi^2}\right),$$

and $$\nabla^4 = \nabla^2\nabla^2, \quad \epsilon = A^{-1} = [\alpha g\tfrac{1}{2}\Delta T a^3/(\kappa\nu)]^{-1},$$

A is the Rayleigh number, $\sigma = \nu/\kappa$ is the Prandtl number, and ν, κ, α, and g are, respectively, the kinematic viscosity, thermal diffusivity, coefficient of cubical expansion, and the Earth's gravity.

We cannot discard the right-hand side of (1) *a priori*. However if we can show that it is indeed small after we have obtained the solutions, we are justified in dropping this term in the analysis. It is certainly negligibly small if the Prandtl number is infinitely large.

Let us assume the total solutions to be of the following form:

$$T = T^{(0)} + \theta = y + \theta = r\sin\phi + \theta, \tag{3}$$

$$\Psi = \psi^{(0)} + \psi, \tag{4}$$

where $T^{(0)}$ is the interior solution, and $\psi^{(0)}$ is some asymptotic value of ψ, and also can be considered as the interior solution. θ and ψ are the boundary-layer corrections. Substituting (3) and (4) into (1) and (2), we have,

$$\epsilon\nabla^4\psi + \cos\phi\frac{\partial\theta}{\partial r} - \sin\phi\, r^{-1}\frac{\partial\theta}{\partial\phi} = 0, \tag{5}$$

$$\nabla^2\theta - \cos\phi\frac{\partial\psi}{\partial r} + \sin\phi\, r^{-1}\frac{\partial\psi}{\partial\phi} = 0, \tag{6}$$

$$\epsilon\nabla^4\psi^{(0)} = O(\epsilon\sigma^{-1}), \tag{7}$$

$$J(\psi^{(0)}, T^{(0)}) = 0. \tag{8}$$

The boundary conditions are: $\partial\psi/\partial r = \psi = 0$, and $\partial\theta/\partial r = -\partial T^{(0)}/\partial r = -\sin\phi$ at $r = 1$. θ and ψ approach some asymptotic values in the interior which are yet to be determined. Equations (7) and (8) both impose constraints on the stream function $\psi^{(0)}$, which we shall discuss next.

4. Solutions of the problem

Equation (8) shows that in the interior, $\psi^{(0)} = \psi^{(0)}[T^{(0)}] = \psi^{(0)}(y)$. In other words, the interior flow, if exists at all, must be parallel to the isotherms. The intuitive explanation is that because the gravitationally stable interior is strongly stratfied as $A \to \infty$, it is difficult for any vertical motion to persist except under very special conditions as we shall see later. The flows are therefore most likely to be horizontal along the isotherms. Another observation is that since $T^{(0)} = y$, $\partial T^{(0)}/\partial x = 0$. Hence $\psi^{(0)}$ is approximately governed by (7). No motion is generated by buoyancy in the interior. Any motion there must be due to some entrainment or detrainment from the boundary layers, which essentially serve as boundary conditions for (7). We shall come back to the discussion of the interior flow again after we have obtained the boundary-layer solutions.

Obviously, there are at least three flow regimes in addition to the flow in the interior. They are, (as shown schematically in figure 1 for the first quadrant): (i) $\phi \neq \frac{1}{2}\pi, r = 1$, (ii) $\phi = \frac{1}{2}\pi, r < 1$, and (iii) $\phi \approx \frac{1}{2}\pi, r = 1$. (i) and (iii) will give boundary layers on the curved surface, and (ii) will give internal boundary layers. We shall consider them separately, and determine precisely the angular span over which the equations governing each flow regime are deemed valid later.

(i) $\phi \neq \frac{1}{2}\pi$ or $\frac{3}{2}\pi, r = 1$, *boundary layer on the cylindrical surface*

In order to obtain boundary-layer solutions, we shall scale (5) and (6) with the stretched coordinate $\eta = \epsilon^{-\frac{1}{4}}(1-r)$. Replace $r^{-1}\partial/\partial\phi$ by $\partial/\partial s$. Since we are considering

the neighbourhood of $r = 1$, we shall assume ∂s to be independent of r. With these transformations, we have

$$\frac{\partial^4 \psi}{\partial \eta^4} - \cos\phi\, \epsilon^{-\frac{1}{4}} \frac{\partial \theta}{\partial \eta} - \sin\phi \frac{\partial \theta}{\partial s} = O(\epsilon^{\frac{1}{2}} \psi_{\eta\eta ss}), \tag{9}$$

$$\epsilon^{-\frac{1}{2}} \frac{\partial^2 \theta}{\partial \eta^2} + \cos\phi\, \epsilon^{-\frac{1}{4}} \frac{\partial \psi}{\partial \eta} + \sin\phi \frac{\partial \psi}{\partial s} = O(\theta_{ss}). \tag{10}$$

For $\phi \neq \frac{1}{2}\pi$, (9) and (10) can be simplified as follows:

$$\frac{\partial^4 \psi}{\partial \eta^4} - \cos\phi \frac{\partial G}{\partial \eta} = O(\epsilon^{\frac{1}{4}}), \tag{11}$$

$$\frac{\partial^2 G}{\partial \eta^2} + \cos\phi \frac{\partial \psi}{\partial \eta} = O(\epsilon^{\frac{1}{4}}), \tag{12}$$

where $\theta = \epsilon^{\frac{1}{4}} G$, with the modified boundary conditions: $\psi = \partial\psi/\partial\eta = 0$ and $\partial G/\partial\eta = -\sin\phi$ at $\eta = 0$. These are similar to the Ekman-boundary equations in rotating fluids (Greenspan 1968). We can readily obtain the following solutions (Quon 1983*a*):

$$\psi = \tan\phi[1 - \exp(-\lambda\eta)(\cos\lambda\eta + \sin\lambda\eta)] + O(\epsilon^{\frac{1}{4}}), \tag{13}$$

$$\theta = \epsilon^{\frac{1}{4}} G = -\epsilon^{\frac{1}{4}} (\sin\phi/\lambda) \exp(-\lambda\eta) \cos\lambda\eta + O(\epsilon^{\frac{1}{2}}), \tag{14}$$

where $\lambda = \cos^{\frac{1}{2}}\phi/\sqrt{2}$.

Equation (13) gives $\tan\phi$ as the asymptotic condition for $\psi(0)$ at $r = 1$. Hence we can deduce the interior solution to be $\psi(0) = +y/(1-y^2)^{\frac{1}{2}}$ which is equal to $\tan\phi$ at $r = 1$. This is consistent with our assumption that $\psi^{(0)} = \psi^{(0)}(y)$. (Note that we can also write $\tan\phi = (1-x^2)^{\frac{1}{2}}/x$ at $r = 1$ as an alternative asymptotic condition. This, however, contradicts our requirement that $\psi^{(0)} = \psi^{(0)}(y)$, although the latter form for $\tan\phi$ is a perfectly good solution if the interior isotherms are vertical!)

We note that in the second quadrant, $\tan\phi < 0$. (Note that in $\lambda = \cos^{\frac{1}{2}}\phi/\sqrt{2}$, $\cos^{\frac{1}{2}}\phi$ comes from $(\cos^2\phi)^{\frac{1}{4}}$, therefore it does not matter whether $\cos\phi$ is positive or negative.) Hence the asymptotic condition is $\psi^{(0)} = -y/(1-y^2)^{\frac{1}{2}}$. Equations (13) and (14) are still valid solutions. This means that, by symmetry, there is a sharp jump in the interior stream function at $\phi = \frac{1}{2}\pi$ between the first and second quadrants. There is no discontinuity in the temperature, because θ asymptotically goes to 0 in the interior. In quadrant 3, $\tan\phi > 0$, but $y < 0$. Therefore $\psi^{(0)} = -y(1-y^2)^{\frac{1}{2}}$ and in quadrant 4, $\psi^{(0)} = y(1-y^2)^{\frac{1}{2}}$. It is obvious that there is also a discontinuity in $\psi^{(0)}$ between the third and fourth quadrants at $\phi = \frac{3}{2}\pi$. However, the interior stream functions are continuous at $y = 0$, for $1 > x > -1$, where ψ is zero. Consequently there is no need for a boundary layer at $y = 0$. In the next section, we shall find ways to smooth over these discontinuities at $x = 0$.

Now we can also check whether $y/(1-y^2)^{\frac{1}{2}}$ satisfies (7). For $|y| < 1$, we can expand $y/(1-y^2)^{\frac{1}{2}} = y + \frac{1}{2}y^3 + \frac{3}{8}y^5 + \ldots$. We have $\epsilon\nabla^4\psi^{(0)} = 0 + O(\epsilon y)$. Hence, $y/(1-y^2)^{\frac{1}{2}}$ satisfies (7) with an error $O(\epsilon y)$ which is bounded for $|y| < 1$. Since $\psi^{(0)} = \psi^{(0)}(y)$, $\epsilon\sigma^{-1} J(\psi^{(0)}, \nabla^2\psi^{(0)}) = 0$, which is the error term in (1). Hence no error is introduced into the interior stream function by neglecting the intertial terms, regardless of the value of σ as long as it is greater than unity!

(ii) $\phi = \frac{1}{2}\pi$ or $\frac{3}{2}\pi, r < 1$, *the internal boundary layer*

When $\phi = \frac{1}{2}\pi$, we shall use the Cartesian coordinates, (x, y) and the relevant equations are

$$\epsilon \frac{\partial^4 \psi}{\partial x^4} - \frac{\partial \theta}{\partial x} = O(\epsilon \psi_{xxyy}), \tag{15}$$

$$\frac{\partial^2 \theta}{\partial x^2} + \frac{\partial \psi}{\partial x} = O(\theta_{yy}). \tag{16}$$

Equations (15) and (16) are valid for the internal boundary layers on both sides of the y-axis. However, the stretching procedure is slightly different in the two half-planes.

(*a*) *First and fourth quadrants*, $x > 0$

Using stretched coordinate $\xi = \epsilon^{-\frac{1}{4}} x$, (15) and (16) become

$$\frac{\partial^4 \psi}{\partial \xi^4} - \epsilon^{-\frac{1}{4}} \frac{\partial \theta}{\partial \xi} = O(\epsilon^{\frac{1}{2}}), \tag{17}$$

$$\epsilon^{-\frac{1}{2}} \frac{\partial^2 \theta}{\partial \xi^2} + \epsilon^{-\frac{1}{4}} \frac{\partial \psi}{\partial \xi} = O(\theta). \tag{18}$$

Note that (17) and (18) are the same as (11) and (12) if we replace $\cos\phi$ in the latter by unity and $\epsilon^{-\frac{1}{4}}\theta$ by G and multiply (18) by $\epsilon^{\frac{1}{4}}$. The solutions are therefore also of Ekman-boundary-layer type, although the dynamical origins of these two distinct boundary layers are different. On the cylindrical surface, the temperature corrections induce a boundary-layer flow, which in turn forces a gentle flow in the interior. Conversely, the discontinuity of the induced interior flow at $x = 0$ generates an internal boundary layer. The resulting temperature perturbation due to this internal boundary layer can thus be viewed as an effect rather than a cause.

Since the stream function is antisymmetric about $x = 0$, we expect the stream function and its second derivative to be zero at $x = 0$. This implies a non-zero and continuous velocity (first -order derivative of ψ) across the vertical axis at $x = 0$. On the other hand, we expect a continuous temperature at $x = 0$. Therefore, we shall impose the following boundary conditions on (17) and (18):

$$\psi = \frac{\partial^2 \psi}{\partial \xi^2} = 0 \quad \text{at} \quad x = 0, \quad \psi \to \psi^{(0)} \quad \text{as} \quad \xi \to \infty,$$

$$\theta \text{ continuous at } x = 0, \quad \theta \to 0 \quad \text{as} \quad \xi \to \infty.$$

Then the solutions are

$$\psi = \psi^{(0)}[1 - \exp(-\xi/\sqrt{2}) \cos(\xi/\sqrt{2})] + O(\epsilon^{\frac{1}{2}}), \tag{19}$$

$$\theta = -\epsilon^{\frac{1}{4}} \psi^{(0)}/\sqrt{2} \exp(-\xi/\sqrt{2}) [\cos(\xi/\sqrt{2}) - \sin(\xi\sqrt{2})] + O(\epsilon^{\frac{1}{2}}), \tag{20}$$

where $\psi^{(0)} y/(1-y^2)^{\frac{1}{2}}$.

(*b*) *Second and third quadrants*, $x < 0$

For $x < 0$, we shall use the stretched coordinate $\xi = -\epsilon^{\frac{1}{4}}x$. Then (15) and (16) become

$$\frac{\partial^4\psi}{\partial\xi^4} + \epsilon^{-\frac{1}{4}}\frac{\partial\theta}{\partial\xi} = O(\epsilon^{\frac{1}{2}}), \tag{21}$$

$$\epsilon^{-\frac{1}{2}}\frac{\partial^2\theta}{\partial\xi^2} - \epsilon^{-\frac{1}{4}}\frac{\partial\psi}{\partial\xi} = O(\theta). \tag{22}$$

If we replace θ by $-\theta$ and (21) and (22), they revert to the form of (17) and (18). Hence the solutions for (21) and (22) are

$$\psi = \psi^{(0)}[1 - \exp(-\xi/\sqrt{2})\cos(\xi/\sqrt{2})] + O\epsilon^{\frac{1}{2}}), \tag{23}$$

$$\theta = \epsilon^{\frac{1}{4}}\psi^{(0)}/\sqrt{2}\exp(-\xi/\sqrt{2})[\cos(\xi/\sqrt{2}) - \sin(\xi/\sqrt{2})] + O(\epsilon^{\frac{1}{2}}), \tag{24}$$

where $\psi^{(0)} = -y/(1-y^2)^{\frac{1}{2}}$.

At $x = 0, \theta = -\epsilon^{\frac{1}{4}}y/(1-y^2)^{\frac{1}{2}}$ from both (20) and (24). Hence θ is continuous at $x = 0$. We also have $\psi = 0$ and $\partial^2\psi/\partial x^2 = 0$ at $x = 0$, which are the imposed boundary conditions. Furthermore

$$\frac{\partial\psi}{\partial x} = \epsilon^{\frac{1}{4}}\frac{\partial\psi}{\partial\xi} = \epsilon^{\frac{1}{4}}/\sqrt{2}\psi^{(0)} = (\epsilon^{\frac{1}{4}}/\sqrt{2})\,y/(1-y^2)^{\frac{1}{2}} \quad \text{at} \quad x = 0 \quad \text{for } y > 0,$$

and

$$\frac{\partial\psi}{\partial x} = -\epsilon^{\frac{1}{4}}\partial\psi/\partial\xi = -\epsilon^{\frac{1}{4}}/\sqrt{2}\psi^{(0)} = -\epsilon^{\frac{1}{4}}\sqrt{2}(-y)/(1-y^2) \quad \text{at} \quad x = 0 \quad \text{for} \quad y < 0$$

from (19) and (23). Therefore, by $\partial\psi/\partial x = u$, the radial velocity (the vertical velocity at $x = 0$) is continuous across $x = 0$.

Except for the polar regions in the neighbourhoods of $\phi = \frac{1}{2}\pi$, and $\frac{3}{2}\pi$ at $r = 1$, we have found solutions for the temperature and stream function over the whole cylinder cross-section. Let us summarize what we have found so far, and estimate what additional solutions may be required in these polar regions to make the solutions complete.

In figure 2(*a*, *b*) we have plotted ψ and θ as functions of r at two values of ϕ in the neighbourhood of $r = 1$. Note that the amplitudes of both ψ and θ are decreasing with decreasing ϕ. This indicates that the larger the boundary slope ($= -\cot\phi$), the weaker the boundary layer. Thus ψ, the mass flux, is detrained into the interior as the flow proceeds from $\phi = \frac{1}{2}\pi$ to 0 (in the first quadrant). It decreases until it has completely emptied itself into the interior at $y = 0$. This efflux from the boundary layer is what creates the slow motion in the interior.

In figure 3(*a*, *b*) we have plotted ψ and θ across the internal layer at $y = \frac{1}{2}$. We see that both functions are continuous at $x = 0$ as required. The temperature has a cusp due to the maximum advection at $x = 0$. The internal layer in fact consists of two boundary layers side by side.

It is now appropriate to establish rigorously how close to the poles the above solutions are valid. We have neglected the last terms in (9) and (10) in comparison with the second terms. Since $\partial\theta/\partial\eta$ and $\partial\theta/\partial s = O(1)$, we must have $\epsilon^{-\frac{1}{4}} \gg \tan\phi$, or $\epsilon^{\frac{1}{4}} \ll \cot(\phi) = \tan(\frac{1}{2}\pi - \phi) = \tan\gamma = \gamma + \gamma^3/3 + \gamma^5/15 + \ldots, \gamma = (\frac{1}{2}\pi - \phi)$. If $\gamma \ll 1$, we can approximate $\tan\gamma$ by γ. Hence for (11) and (12) to be valid approximations to (9) and (10), we must have $\epsilon^{\frac{1}{4}} \ll \gamma$. For example we can require $\gamma = 10\epsilon^{\frac{1}{4}}$. If we assume

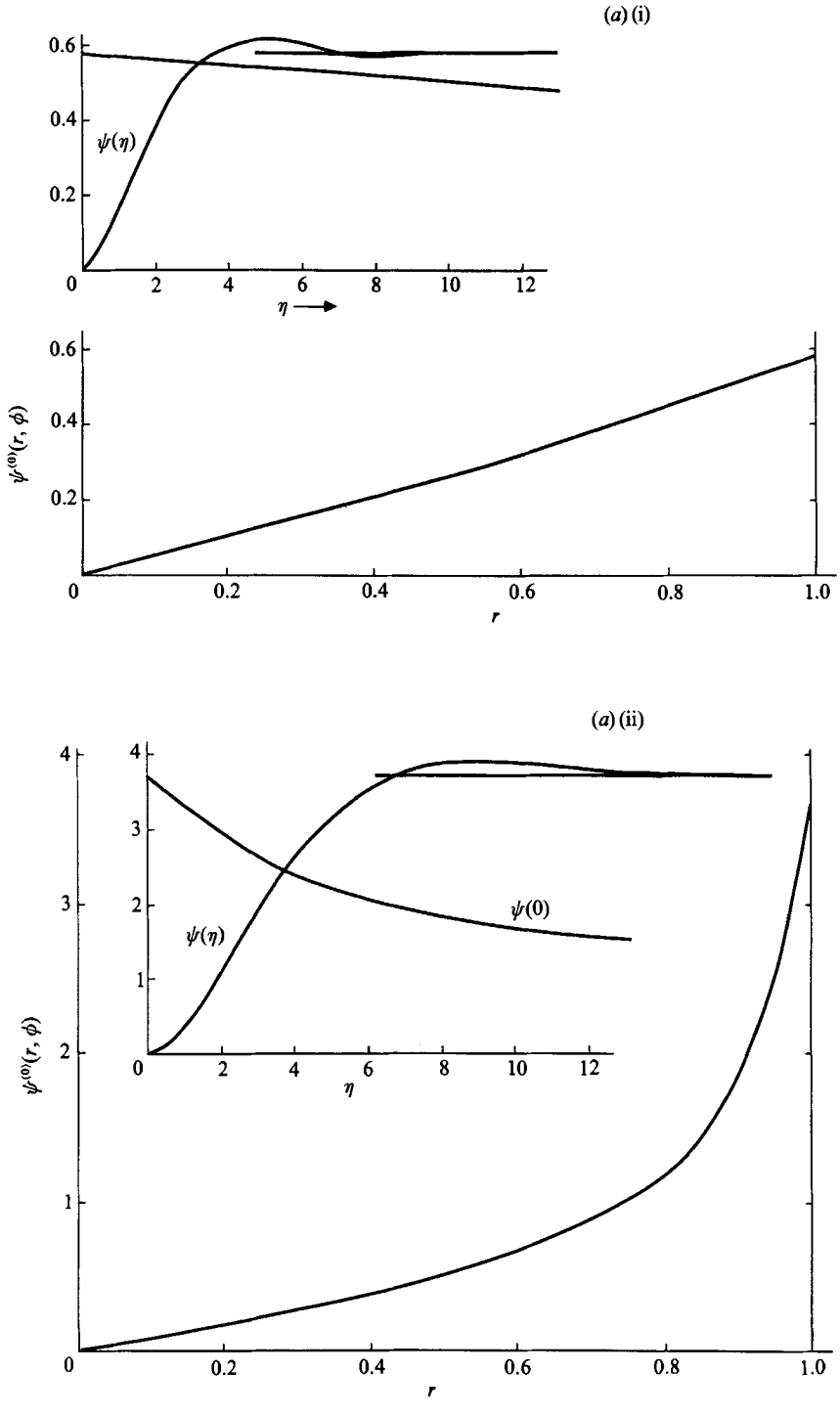

FIGURE 2(a). For caption see facing page.

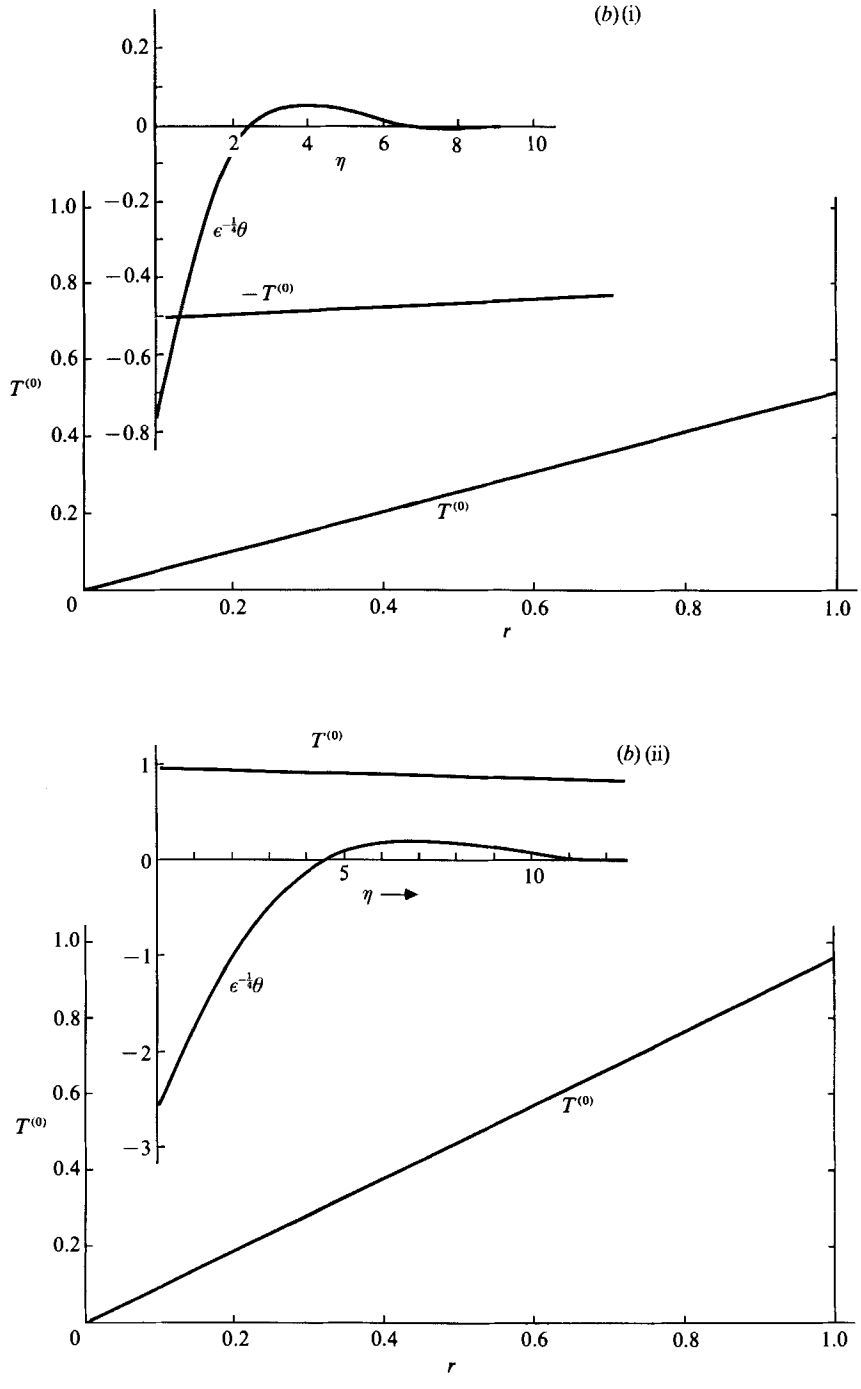

FIGURE 2. (*a*) ψ as a function of r at:(i) $\phi = 30°$, (ii) $\phi = 75°$; $\psi^{(0)} = r\sin\phi/(1-r^2\sin^2\phi)^{\frac{1}{2}}$. (*b*) θ as a function of r at: (i) $\phi = 30°$, (ii) $\phi = 75°$; $T^{(0)} = r\sin\phi$.

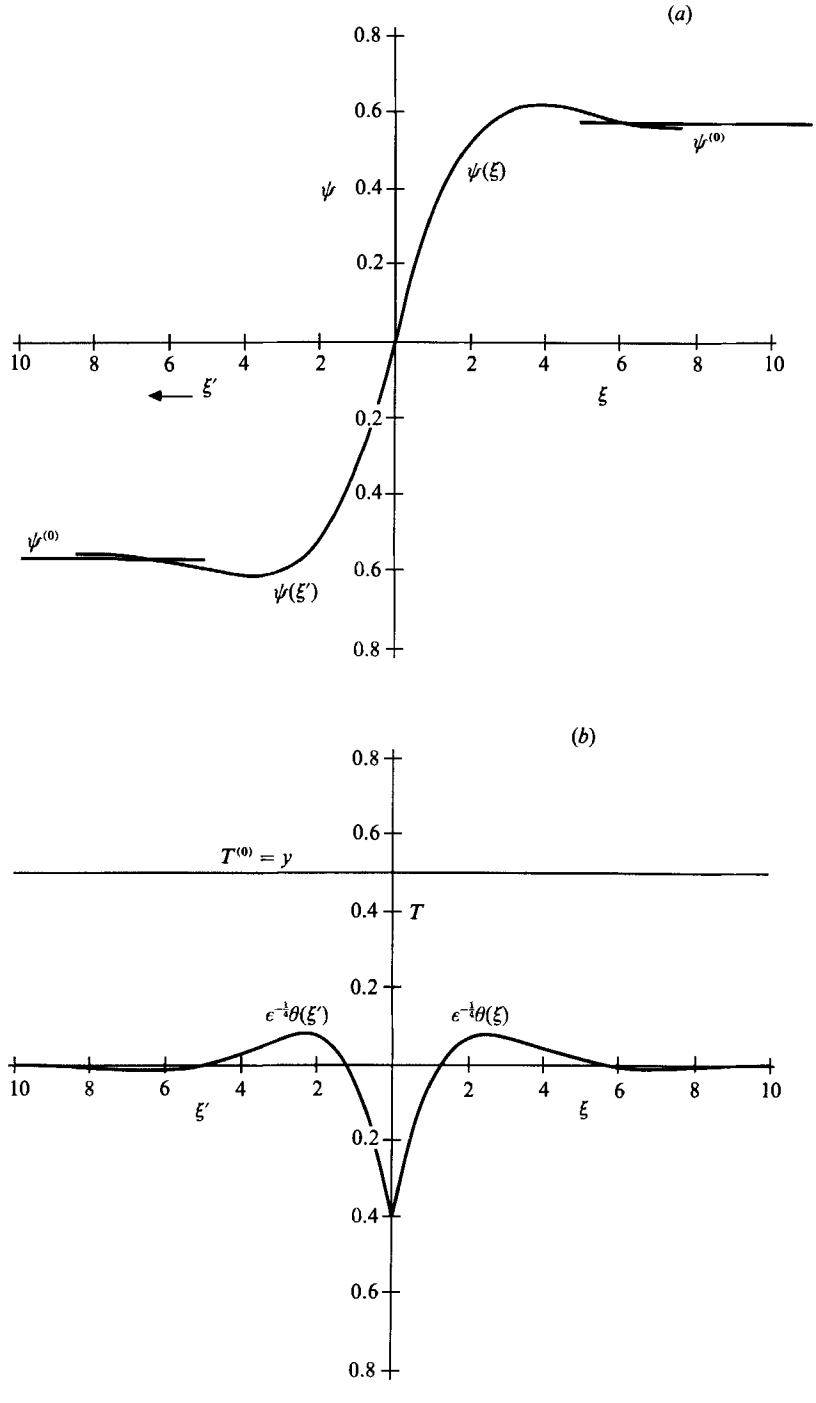

FIGURE 3. (*a*) ψ across the internal layer at $y = \frac{1}{2}$; $\psi^{(0)} = -y/(1-y^2)^{\frac{1}{2}}$. (*b*) θ across the internal layer at $y = \frac{1}{2}$; $\xi = \epsilon^{-\frac{1}{4}}x$, $\xi' = -\epsilon^{-\frac{1}{4}}x$.

$\epsilon = 10^{-8}$, then we cannot use the solutions within an angle of 0.1 rad, or 5.73° of the poles. What this means is that the internal boundary layer is valid up to $y = \sin 84.27° = 0.995$. At this value of y, the interior stream function is tan 84.27° = 9.97, and the non-dimensional horizontal velocity is $\partial\psi/\partial y = 89.24$. If we use $\kappa = 1.4 \times 10^{-3}$ cm^2/s, and $a = 7$ cm, as used in Kimura & Bejan (1980*a*), then the characteristic velocity is 2.0×10^{-4} cm/s. The above velocity is 1.78×10^{-2} cm/s, which is about one tenth of the observed axial velocity. If we calculate the maximum velocity in the boundary layer from (13) at $\lambda\eta = \frac{3}{4}\pi$, i.e. $v = -\partial\psi/\partial r = -\epsilon^{-\frac{1}{4}}\partial\psi/\partial\eta$, we have $v = -2.30\,\epsilon^{-\frac{1}{4}} = -230$, corresponding to a dimensional velocity about 4.60×10^{-2} cm/s, about one quarter the axial speed observed by Kimura & Bejan (1980*a*). Also note that our Rayleigh number is one sixteenth of that defined by Kimura & Bejan for the same set of parameters. In the vicinity of the poles, there are other mechanisms that will alter the flow somewhat. We shall study this possibility next.

(iii) $\phi \approx \frac{1}{2}\pi$ or $\frac{3}{2}\pi, r = 1$, *boundary layer at the poles*

In Quon (1983*a*, Case 2, p. 635), the case for $\phi = \frac{1}{2}\pi$, has an almost one-to-one correspondence to the situation here. When $\phi = \frac{1}{2}\pi$, (5) and (6) become

$$\epsilon\nabla^4\psi - r^{-1}\frac{\partial\theta}{\partial\phi} = 0, \tag{25}$$

$$\nabla^2\theta + r^{-1}\frac{\partial\psi}{\partial\phi} = 0. \tag{26}$$

We are considering $r \approx 1$. We shall make the following substitution:

$$r\,\mathrm{d}\phi = \mathrm{d}s, \quad \tfrac{1}{2}\pi > s > 0, \quad \mu = \epsilon^{\frac{1}{2}}, \quad \theta = \mu\chi,$$

to obtain

$$\mu\nabla^4\psi = \frac{\partial\chi}{\partial s}, \tag{27}$$

$$\mu\nabla^2\chi = -\frac{\partial\psi}{\partial s}. \tag{28}$$

As discussed in Quon (1983*a*), and more thoroughly in Stewartson (1957) and Greenspan (1968), (27), and (28) can take a single $\mu^{\frac{1}{3}}$ layer or $\mu^{\frac{1}{3}}$ and $\mu^{\frac{1}{4}}$ double layers. The criterion for using a single layer or double layers depends on whether χ is a symmetric or antisymmetric function of s. If χ is symmetric about $s = 0$, ψ is antisymmetric and vice versa. By replacing $s/\pi = (\frac{1}{2} - z)$ in Quon (1983*a*, equations (33′) and (34′)) (this substitution is necessary to give non-zero asymptotic values for the internal boundary layer extension to match onto at $s = \frac{1}{2}\pi$ as shown below), we have, using superscript (iii) to identify the area of validity,

$$\psi^{(\mathrm{iii})} = \left(\frac{2}{\mu}\right)^{\frac{1}{4}}\frac{s}{\pi}\exp(-2^{\frac{1}{4}}\zeta_1) + \frac{1}{\pi}\left(\frac{2}{\mu}\right)^{\frac{1}{4}}\sum_{m=1}^{\infty}\frac{(-)^m}{m}\sin\left[\sigma_m^3\left(\frac{s}{\pi}\right)\right]$$
$$\times\left[\exp(-\sigma_m\zeta_2) - 2\exp(-\tfrac{1}{2}\sigma_m\zeta_2)\cos\left(\frac{\sqrt{3}}{2}\sigma_m\zeta_2\right)\right] + O(\mu^{-\frac{1}{6}}), \tag{29}$$

$$\chi^{(\mathrm{iii})} = +(2\mu^3)^{-\frac{1}{4}}\exp(-2^{\frac{1}{4}}\zeta_1) + (2^{\frac{5}{4}}\mu^{-\frac{7}{12}})\sum_{m=1}^{\infty}\frac{(-)^m}{\sigma_m^2}\cos\left[\sigma_m^3\left(\frac{s}{\pi}\right)\right]$$
$$\times\left[\exp(-\sigma_m\zeta_2) - 2\exp(-\tfrac{1}{2}\sigma_m\zeta_2)\cos\left(\frac{\sqrt{3}}{2}\sigma_m\zeta_2 + \tfrac{2}{3}\pi\right)\right] + O(\mu^{-\frac{1}{2}}), \tag{30}$$

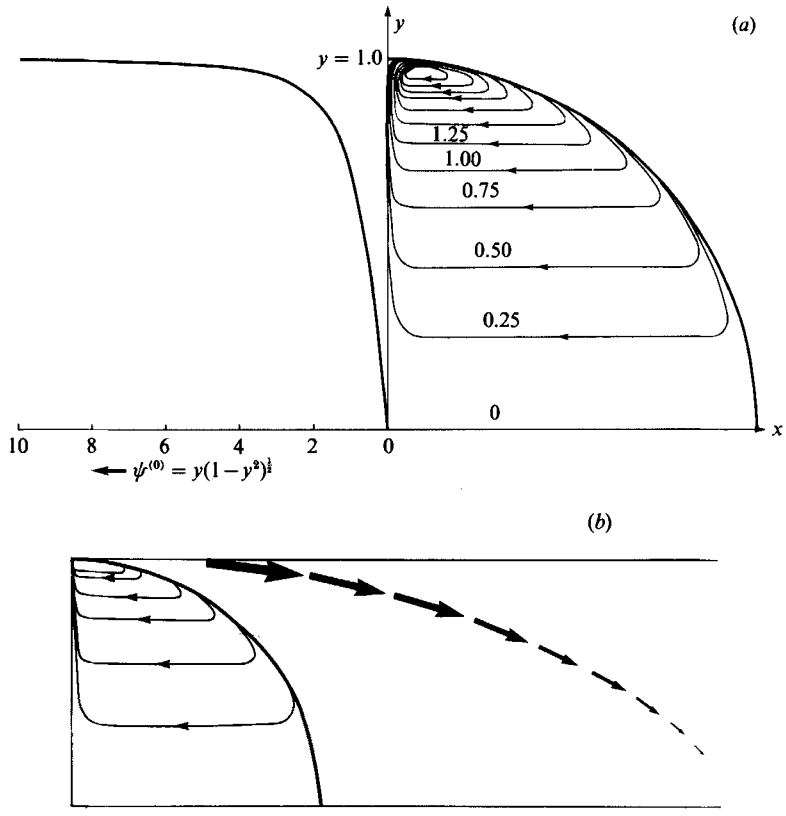

FIGURE 4. (*a*) Schematic of composite cross-sectional flows and $\psi^{(0)}$ as a function of y in the first quadrant. (*b*) Possible helical flows on the inner surface of the cylinder.

where $\zeta_1 = \mu^{-\frac{1}{4}}(1-r)$, $\zeta_2 = \mu^{-\frac{1}{3}}(1-r)$, and $\sigma_m^3 = 2m\pi$. Therefore the two boundary-layer thicknesses are $O(\mu^{-\frac{1}{3}})$ and $O(\mu^{-\frac{1}{4}})$ respectively.

If we substitute (29) and (30) into (27) and (28), we see that they do indeed satisfy the equations, to their respective order of accuracy. We can also see that they satisfy the boundary conditions $\psi^{(\mathrm{iii})} = \partial\psi^{(\mathrm{iii})}/\partial r = 0$, and $\mu\,\partial\chi^{(\mathrm{iii})}/\partial r = -1$ at $r = 1$. Furthermore, $\chi \to 0$ as $\zeta_1, \zeta_2 \to \infty$. However, in order for $\psi^{(\mathrm{iii})} = 0$ to hold at $r = 1$, we must have

$$\frac{s}{\pi} = \frac{2}{\pi}\sum_{m=1}^{\infty}\frac{(-)^m}{m}\sin\left[\sigma_m^3\left(\frac{s}{\pi}\right)\right].$$

This is valid only for $|s| < \frac{1}{2}\pi$ which is always satisfied in the neighbourhood of the poles. Now, we need to match $\psi^{(\mathrm{iii})}$ onto the interior stream function at some y, or at some value of ζ_2. The matching is clearly possible at $(1-r) < \mu^{\frac{1}{4}}$ where $\psi^{(\mathrm{iii})} \approx \mu^{-\frac{1}{4}}$. This somewhat convoluted procedure of matching near $\phi = \frac{1}{2}\pi$ is necessary mainly because the interior solution, $\tan\phi$, which is valid for $\phi < \frac{1}{2}\pi$, is undefined at $\phi = \frac{1}{2}\pi$. Therefore there is no interior solution to match onto at $\zeta_{1,2} = 0$ asymptotically. The function of the $\mu^{\frac{1}{4}}$ layer is to serve as asymptotic condition for the $\mu^{\frac{1}{3}}$ inner layer, and thus help the latter to satisfy the boundary condition at $r = 1$. Note that both $\psi^{(\mathrm{iii})}$ and $\chi^{(\mathrm{iii})} \to 0$ as $\zeta_1, \zeta_2 \to \infty$. In the second quadrant, we shall replace (s/π) by $-(s/\pi)$ in (29). Hence $\psi^{(\mathrm{iii})}$ changes sign. In order to smooth the discontinuity between $\psi^{(\mathrm{iii})}$ on both sides of the y-axis, we need the extension of

the interior boundary layer of the following form (see Quon 1983*a*, equation (35*a*, *b*) and (36)):

$$\psi^{(\mathrm{ii})} = \pm C(\zeta_1)\,[1-\exp(-\xi/\sqrt{2})\cos(\xi/\sqrt{2}), \tag{31a, b}$$

$$\chi^{(\mathrm{ii})} = \mu^{-\frac{1}{2}}\sqrt{2}C(\zeta_1)\,[1-\exp(-\xi/\sqrt{2})\,[\cos(\xi/\sqrt{2})-\sin(\xi/\sqrt{2})], \tag{32}$$

where $C(\zeta_1) = (8\mu)^{-\frac{1}{4}}\exp(-2^{\frac{1}{4}}\zeta_1)$. The superscript (ii) designates the area of extension in the internal layer.

Obviously these solutions match onto the leading terms of $\psi^{(\mathrm{iii})}$ and $\chi^{(\mathrm{iii})}$ as $\xi \to \infty$ and they go to 0 as $\zeta_1 \to \infty$, and therefore they contribute nothing to the internal layer in the fluid interior. One can do similar matching for the boundary layers on the curved surface. It suffices to know that the possibility exists. More importantly, the $\mu^{\frac{1}{3}}$ layer is sufficiently strong to enable the mass flux in the two separated $\epsilon^{\frac{1}{4}}$ layers to communicate with each other. In figure 4(*a*) we have sketched a rough diagram to show the composite flows in the first quadrant. If two jets of axial flows are added, one can visualize the possible helical flows on the cylindrical surface as illustrated in figure 4(*b*).

5. Mechanism of boundary-layer entrainment and detrainment

Physically it is quite clear why the boundary-layer detrainment from the cylindrical surface is necessary. We have shown that the boundary layer flux of a sloping surface is inversely proportional to the absolute value of its slope. The flux has to leak out as the slope of the curved surface increases from 0 to ∞ as ϕ changes from $\frac{1}{2}\pi$ or $\frac{3}{2}\pi$ to $\phi = 0$ or π. Dynamically, both the detrainment and entrainment are equivalent to the Ekman suction in a rotating fluid. This can be shown mathematically as follows.

For ease of algebraic manipulation, we shall consider the entrainment of the internal boundary layer. The influx into this boundary layer will be equal to the efflux from the opposite boundary layer on the curved surface at the same y-level. We shall start with (16) in Cartesian coordinates (x, y) with the corresponding velocity components $(\hat{u} = -\partial\psi/\partial y, \hat{v} = \partial\psi/\partial x)$, and the continuity equation $\partial\hat{u}/\partial x + \partial\hat{v}/\partial y = 0$:

$$\frac{\partial^2\theta}{\partial x^2} + \frac{\partial\psi}{\partial x} = 0.$$

Differentiating the above equation with respect to y once, replacing x in the first term with stretched coordinate $x = \epsilon^{\frac{1}{4}}\xi$ and making use of the continuity equation in the second term, we have

$$\frac{\partial^3\theta}{\partial y\,\partial x^2} + \frac{\partial^2\psi}{\partial x\,\partial y} = \epsilon^{-\frac{1}{2}}\frac{\partial^3\theta}{\partial y\,\partial\xi^2} - \frac{\partial\hat{u}}{\partial x} = 0.$$

Integrating the above equation once with respect to x, we have

$$\int_0^{x_0}\frac{\partial\hat{u}}{\partial x}\,\mathrm{d}x = \epsilon^{-\frac{1}{2}}\frac{\partial}{\partial y}\int_0^{\infty}\frac{\partial^2\theta}{\partial\xi^2}\epsilon^{\frac{1}{4}}\,\mathrm{d}\xi,$$

as $x \to x_0, \xi \to \infty, x_0$ being some value of x just outside the boundary layer. Then,

$$(\hat{u}(x_0) - \hat{u}(0)) = \epsilon^{-\frac{1}{4}}\frac{\partial}{\partial y}\left[\frac{\partial\theta}{\partial\xi}\right]_{\xi=0}^{\xi=\infty},$$

θ being given by the boundary-layer solution in (20). Since $\hat{u}(0) = 0$, we obtain

$$\hat{u}(x_0) = -\epsilon^{-\frac{1}{4}} \frac{\partial \psi^{(0)}}{\partial y} \frac{\epsilon^{\frac{1}{4}}}{\sqrt{2}} \left[-\sqrt{2} \exp\left(-\frac{\xi}{\sqrt{2}}\right) \cos\left(\frac{\xi}{\sqrt{2}}\right) \right]_0^\infty = -\frac{\partial \psi^{(0)}}{\partial y}.$$

Therefore the suction velocity is the same as the interior velocity. (One can as readily obtain the suction velocity by integrating the continuity equation directly.) Clearly if $\psi^{(0)} =$ constant, there would be no entrainment or detrainment. Recall that the variation in $\psi^{(0)}(y)$ arises from the fact that the cylindrical surface is curved. If it were a linear surface, it would have a constant slope which is equal to $-\cot\theta$, and $\psi^{(0)} = \tan\theta =$ constant (Wunsch 1970; Phillips 1970; Quon 1976, 1983*a*).

6. Discussion

We have studied the cross-sectional flows in an insulated cylinder differentially heated on the two endwalls at high Rayleigh number. The assumption of two-dimensionality of the secondary cross-sectional flows may not hold exactly, and the zero-order temperature distribution in the vertical may vary somewhat from linearity when the Rayleigh number and the aspect ratio of the cylinder L/a, L being the length, are not sufficiently large. The fundamental mechanism and the basic structure of the boundary layers are quite clear. Some aspects of the boundary-layer flows ought to be visible in laboratory experiments, if, as we have shown, it is as large as a quarter the speed of the axial flow for $A = 10^8$.

One should also take into consideration these boundary-layer structures when designing three-dimensional numerical experiments. Reasonably fine grids are required to resolve these boundary layers. Quon (1983*b*) has thoroughly discussed the effects of grid spacings on the numerical computations of high-Rayleigh-number convection in two dimensions.

REFERENCES

Batchelor, G. B. 1954 Heat transfer by free convection across a closed cavity between vertical boundaries at different temperatures. *Q. Appl. Maths* **12**, 209–233.

Bejan, A. Al-Homoud, A. A. & Imberger, J. 1981 Experimental studies of high-Rayleigh-number convection in a horizontal cavity with different end temperatures. *J. Fluid Mech.* **109**, 283–299.

Bejan, A. & Tien, C. L. 1978 Fully developed natural counterflow in a long horizontal pipe with different end temperatures. *Intl J. Heat Mass Transfer* **21**, 701–708.

Cormack, D. E., Leal, L. G. & Imberger, J. 1974*a* Natural convection in a shallow cavity with differentially heated end walls. Part 1. Asymptotic theory. *J. Fluid Mech.* **65**, 209–229.

Cormack, D. E., Leal, L. G. & Seinfeld, J. H. 1974*b* Natural convection in a shallow cavity with differentially heated end walls. Part 2. Numerical solutions. *J. Fluid Mech.* **65**, 231–246.

Elder, J. W. 1965 Laminar free convection in a vertical slot. *J. Fluid Mech.* **23**, 77–98.

Gill, A. E. 1966 The boundary layer regime for convection in a rectangular cavity. *J. Fluid Mech.* **26**, 515–536.

Greenspan, H. P. 1968 *The Theory of Rotating Fluids.* Cambridge University Press.

Hong, S. W. 1977 Natural convection in horizontal pipes. *Intl J. Heat Mass Transfer* **20**, 685–691.

Imberger, J. 1974 Natural convection in a shallow cavity with differentially heated end walls. Part 3. Experimental results. *J. Fluid Mech.* **65**, 247–260.

Kimura, S. & Bejan, A. 1980*a* Experimental study of natural convection in horizontal cylinder with different end temperatures. *Intl J. Heat Mass Transfer* **23**, 1117–1126.

KIMURA, S. & BEJAN, A. 1980*b* Numerical study of natural circulation in a horizontal duct with different end-temperatures. *Wärme-und Stoffübertraguug* **14**, 269–280.

PHILLIPS, O. M. 1970 On flows induced by diffusion in a stably stratified fluid. *Deep-Sea Res.* **17**, 435–443.

QUON, C. 1972 High Rayleigh number convection in an enclosure – a numerical study. *Phys. Fluids* **15**, 12–19.

QUON, C. 1976 Diffusivity induced boundary layers in a tilted square cavity: a numerical study. *J. Comp. Phys.* **22**, 459–485.

QUON, C. 1983*a* Convection induced by insulated boundaries in a square. *Phys. Fluids* **26**, 632–637.

QUON, C. 1983*b* Effects of grid distribution on the computation of high Rayleigh number convection in a differentially heated cavity. In *Numerical Properties and Methodologies in Heat Transfer* (ed. T. M. Shih), pp. 261–281. Hemisphere and Springer.

SCHIROKY, G. H. & ROSENBERGER, F. 1984*a* Free convection of gases in a horizontal cylinder with differentially heated end walls. *Intl J. Heat Mass Transfer* **27**, 587–598.

SCHIROKY, G. H. & ROSENBERGER, F. 1984*b* High Rayleigh number heat transfer in a horizontal cylinder with adiabatic wall. *Intl J. Heat Mass Transfer* **27**, 630–633.

SHIH, T. H. 1981 Computer extended series: natural convection in a long horizontal pipe with different end temperatures. *Intl J. Heat Mass Transfer* **24**, 1295–1303.

SIMPKINS, P. G. & CHEN, K. S. 1986 Convection in horizontal cavities. *J. Fluid Mech.* **166**, 21–39.

SIMPKINS, P. G. & DUDDERAR, T. D. 1981 Convection in rectangular cavities with differentially heated end walls. *J. Fluid Mech.* **110**, 433–456.

SMUTEK, C., BONTOUX, P., ROUX, B., SCHIROKY, G. H., HURFORD, A. C., ROSENBERGER, F. & VAHL DAVIS, G. DE 1985 Three-dimensional convection in horizontal cylinders: numerical solutions and comparisons with experimental and analytical results. *Num. Heat Transfer* **8**, 623–631.

STEWARTSON, K. 1957 On almost rigid rotation. *J. Fluid Mech.* **3**, 17–26.

VAHL DAVIS, G. DE 1983 Natural convection of air in a square cavity: a bench mark numerical solution. *Intl J. Comp. Meth. in Fluids* **3**, 249–264.

VAHL DAVIS, G. DE & JONES, I. P. 1983 Natural convection in a square cavity: a comparison exercise. *Intl J. Comp. Meth. in Fluids* **3**, 227–248.

WUNSCH, C. 1970 On oceanic boundary mixing. *Deep-Sea Res.* **17**, 293–301.